International Journal of Mass Spectrometry 280 (2009) 101–106

Contents lists available at ScienceDirect

International Journal of Mass Spectrometry

journal homepage: www.elsevier.com/locate/ijms

Electron-impact ionization of the $SiCl_3$ radical

M. Gutkin[a,b], J.M. Mahoney[a,1], V. Tarnovsky[a], H. Deutsch[c], K. Becker[a,*]

[a] Department of Physics and Engineering Physics, Stevens Institute of Technology, Hoboken, NJ 07030, USA
[b] Institut für Ionenpysik und Angewandte Physik, Leopold-Franzens Universität, A-6020 Innsbruck, Austria
[c] Institut für Physik, Ernst-Moritz-Arndt Universität, D-17489 Greifswald, Germany

ARTICLE INFO

Article history:
Received 29 May 2008
Received in revised form 29 July 2008
Accepted 31 July 2008
Available online 8 August 2008

Keywords:
Electron-impact ionization
Silicon chloride
Cross section measurement
Fast-beam technique

ABSTRACT

We describe improvements to the fast-beam apparatus that has been used extensively for electron-impact ionization cross section measurements for atoms, molecules, and free radicals in our group for the past 15 years. A high-intensity, dispenser-type electron emitter capable of producing an electron beam of more than 2 mA at electron energies above 50 eV is used instead of a conventional indirectly heated, oxide-coated electron source. We also replaced the channel electron multiplier by a position-sensitive, triple multi-channel plate ion detector. Experiments using well-established ionization cross sections in conjunction with extensive ion trajectory simulations were carried out to verify the performance of the modified fast-neutral-beam apparatus. This apparatus was subsequently employed in the measurement of absolute partial cross sections for the formation of various singly charged positive ions produced by electron impact on $SiCl_3$ for impact energies from threshold to 200 eV. A comparison with calculations and with the previously reported ionization cross section for $SiCl_4$, $SiCl_2$, and SiCl is also made.

1. Introduction

Electron-driven collisional interactions, such as the electron-impact ionization and dissociative ionization of a molecule are of interest from a basic science perspective as well as from the viewpoint of data needs for applications. Rigorous calculations of electron-impact cross sections for molecular ionization are beyond the capabilities of quantum mechanical, first principles methods [1], because of the complexity of the molecular target and the variety of final states in the ionization process. Semi-rigorous methods such as semi-classical and semi-empirical methods are commonly used instead [2]. Even though experimental ionization studies have been carried out for almost 100 years, there are still many atoms, molecules, and free radicals for which no ionization cross section data are available. The reliable determination of partial ionization cross sections presents a particular challenge. Mass- and energy-dispersive elements have to be used to separate singly from multiply charged ions and parent ions from fragment ions. The complete extraction of the product ions from the interaction region, where the electron beam intersects the target beam ('ion source'), the transport of the product ions through the mass- and/or energy-dispersive elements (particularly of fragment ions produced with excess kinetic energy) and their detection with 100% efficiency pose serious challenges.

The group of Märk and co-workers [3] were the first to investigate systematically the ion extraction from the ion source and the ion transport through a mass spectrometer from the ion source to the ion detector. They identified discrimination effects as the most serious problem for accurate absolute partial ionization cross section measurements, particularly in the case of dissociative ionization processes. Detailed investigations of the ion extraction efficiency as a function of excess kinetic energy and of the ion transport efficiency from the ion source to the detector in conjunction with ion trajectory simulations are nowadays essential in characterizing and quantifying the ability of a particular experimental technique and apparatus to determine reliable absolute partial electron-impact ionization cross sections.

Conventional techniques for the measurement of electron-impact ionization cross sections use an effusive gas jet or a heated oven to produce the target beam. These approaches limit the list of targets to stable atoms and molecules. In contrast, the fast-neutral-beam method, which was first introduced by Cook and Peterson [4] and which was subsequently employed extensively by Freund and co-workers [5], has been shown to be a reliable experimental method for the determination of electron-impact ionization cross sections of free radicals and other short-lived and/or unstable species (as well as for atoms and stable molecules). A slightly modified version of this apparatus was subsequently used in our group in a series of absolute ionization cross section measurements for many

* Corresponding author. Present address: Department of Physics, Polytechnic Institute of New York University, Six MetroTech Center, Brooklyn, NY 11201, USA. Tel.: +1 718 260 3608.
E-mail address: kbecker@poly.edu (K. Becker).
[1] Present address: UV Solutions, Newark, NJ 07103, USA.

1387-3806/$ – see front matter © 2008 Elsevier B.V. All rights reserved.
doi:10.1016/j.ijms.2008.07.032

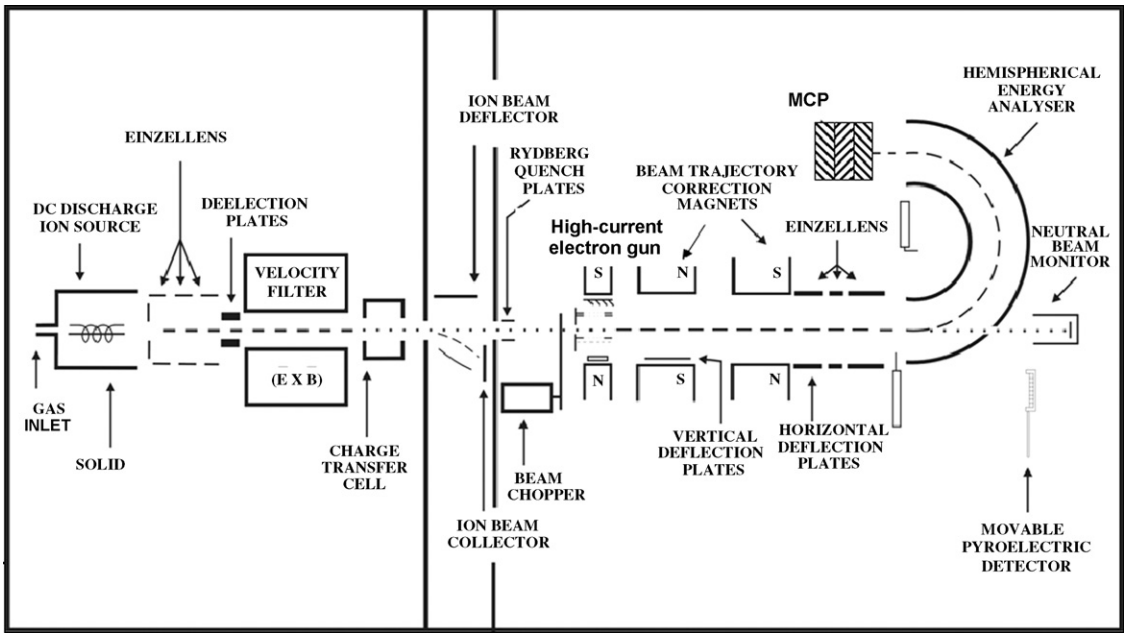

Fig. 1. Schematic diagram of the modified fast-beam apparatus, which employs (i) a positive-sensitive triple-stack multi-channel plate (MCP) detector and (ii) a new dispenser-type high-current electron gun.

molecules and free radicals (see Ref. [6] and references therein to earlier work). Recent advances in experimental techniques made it possible to improve the performance of this apparatus significantly by (i) increasing the electron current density by more than a factor of 20 using a new dispenser-type electron emitter and by (ii) employing position-sensitive ion detection, which allows the determination of the product ion distribution on the face of the detector.

The impact of these improvements and the expanded capabilities of the modified fast-beam apparatus are described in this paper along with the results of a detailed study of the electron-impact ionization of the $SiCl_3$ free radical, which will be discussed also in the context of previously published electron-impact ionization data for $SiCl_2$ and SiCl [7] and for the stable $SiCl_4$ molecule [6] as well as with calculated cross sections. The work on the interactions of $SiCl_x$ ($x = 1–4$) with electrons is largely motivated by the importance of $SiCl_4$ as the main volatile etch product in chlorine-based etching of silicon [8–11]. Furthermore, $SiCl_4$ is used as an admixture in processing plasma feed gas mixtures that are used for selective reactive ion etching of GaAs on AlGaAs [12] and for other plasma-enhanced processes, including the formation of self-assembled nanocrystalline silicon dots by $SiCl_4/H_2$ plasma-enhanced chemical vapor deposition [10] and the characterization of polyester fabrics treated in $SiCl_4$ plasmas [13,14]. The electron-impact ionization and dissociative ionization cross sections of the $SiCl_4$ molecule, as well as of the $SiCl_x$ ($x = 1–3$) reactive species resulting from the collisional break-up of $SiCl_4$, are very important quantities for the understanding and modeling of the interaction of silicon–chlorine plasmas with materials in those applications. We note that some of results described in this paper have been reported earlier at a conference [15].

2. Experimental apparatus and performance verification

2.1. Apparatus modifications

The fast-neutral-beam apparatus used in the present experiments has been described in detail in earlier publications [5,16]. Here we only give a brief summary of two recent modifications to the apparatus and their impact on the performance of the apparatus (see Fig. 1). First of all, we replaced the channel electron multiplier (CEM), which served as ion detector with a position-sensitive, triple multi-channel plate (MCP) detector in a Z-stack arrangement for maximum gain (RoentDek model DLD40 MCP detector with a delay-line anode capable of high-resolution 2D-imaging and fast timing for charged particle or photon detection at high rates with multi-hit capability). The new detector allows us to monitor the distribution of the product ions that emerge from the hemispherical analyzer on the face of ion detector. The ability to obtain the product ion distribution in addition to the total ion count is important in situations where fragment ions that are close in their mass-to-charge ratio are formed with broad excess kinetic energy distributions, which causes the individual ion distributions to overlap on the face of the detector. This was the case in our ionization studies of NO, NO_2, and N_2O, where we could not resolve the ion signals corresponding to N^+ and O^+ and only reported a cross sections for the combined ($N^+ + O^+$) formation [17]. The experimental determination of the ion distribution on the detector face in conjunction with SIMION ion trajectory simulations allow us to deconvolute such overlapping ion distributions and obtain individual cross sections in the modified apparatus.

Secondly, we installed a new electron gun with a dispenser-type cathode, which consists of a porous tungsten matrix of about 20% porosity as a base, interspersed uniformly with a mixture of barium and calcium aluminate as the electron emitting material. The porous metal matrix acts as a reservoir from which the emitting material can diffuse to the surface, maintain an active layer and provide a low work-function surface for the thermionic emission of electrons. The cathode is activated by indirect heating. The new emitter has the following properties:

- 1–2 A/cm^2 continuous emission current density;
- a useful lifetime of more than 10,000 h;
- no degradation of the emission current over time;
- a minimal evaporation rate;
- superior shock and vibration resistance;

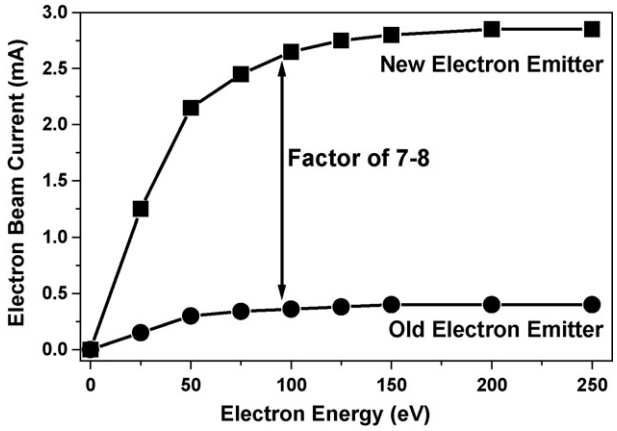

Fig. 2. Comparison of the electron beam current vs. electron energy for the new electron emitter (squares) and the old electron emitter (circles).

- high reliability and reproducibility of the operating characteristics.

The total beam current produced by the new electron emitter is almost a factor of 10 higher than what was obtained with the previous gun. A maximum beam current of well over 2 mA at energies above 50 eV can be achieved (Fig. 2). At beam energies of 10 eV and 4 eV, the total current is still around 20 μA and 5 μA, respectively. In addition, the size (i.e., cross section) of the electron beam produced by the new emitter in the interaction region is about 0.2 cm^2 compared to a beam size of 0.6 cm^2 produced by the old electron gun. Thus, the current density produced by the new emitter of up to 25 mA/cm^2 (for dc operation) exceeds that of the old gun by about a factor of 20. We note that, in principle, even higher currents, up to 4 mA can be realized with this new electron emitter for impact energies above about 70 eV, but we usually limited the current used in our experiments to less than 2 mA at energies above 50 eV in an effort to minimize distortion of the shape of the electron beam in the interaction region due to space charge effects.

All other features and components of the original fast-beam apparatus and the experimental procedure to obtain absolute cross sections as described earlier [5,16] remained unchanged. In principle, the fast-beam apparatus affords the capability to measure directly all quantities that determine the absolute cross section. However, here we used the well-established Kr or Ar absolute ionization cross sections to calibrate a pyroelectric crystal. The calibrated crystal, in turn, was then used to determine the flux of the neutral target beam in absolute terms. The typical uncertainty of absolute ionization cross sections determined in the fast-beam apparatus is in the range from ±15% to ±18% [5,16].

2.2. Ion trajectory simulations

We carried out extensive ion trajectory simulations using the most recent version of the SIMION charged particle trajectory simulation package [18] in an attempt characterize and quantify the ion transport, ion collection, and ion detection capabilities of the modified fast-beam apparatus. The simulations track ions formed in the interaction region of the electron beam and the neutral target beam (ion source) to the MCP detector. The electron-induced ionization in the interaction region creates product ions, which in the case of molecular targets consist of parent ions and fragment ions produced by dissociative ionization. Parent ions are formed with essentially the same kinetic energy as the incident neutral beam and no appreciable access kinetic energy is imparted on a parent ion in the ionization process. Fragment ions, on the other hand, are produced with a distribution of access kinetic energies, which may range from thermal and near-thermal to more than 10 eV per fragment ion. As a result, the fragment ions have a much wider kinetic energy spread compared to the parent ions. This, in turn, results is a much more divergent fragment ion beam. Furthermore, the two (or more) fragments formed in the dissociative ionization process share the initial kinetic energy, so that fragment ions travel with less than the initial neutral beam energy towards the detector.

In our simulations, we first create a randomized set of values of the excess kinetic energy for a given fragment ion in a range of values for the excess energy that is either known from other experiments or from the literature. The energy is then converted to a velocity of the fragment, whose direction is randomly selected within a 360° cone. The path of each ion is tracked from the ion source through the electrostatic Einzel lens and the hemispherical analyzer. We also take into account the displacement of the ions due to the small transverse collimating magnetic field and the effect of the additional magnetic steering field (see Fig. 1). Ions that leave the hemispherical analyzer travel an additional few centimeters before they reach the MCP detector (with an active detection area measuring 46 mm in diameter), which is held at a negative potential of 3 kV. The simulation ultimately determines the number of ions arriving at the detector and their position on the detector surface and calculates the transmission percentage. If an ion is lost between

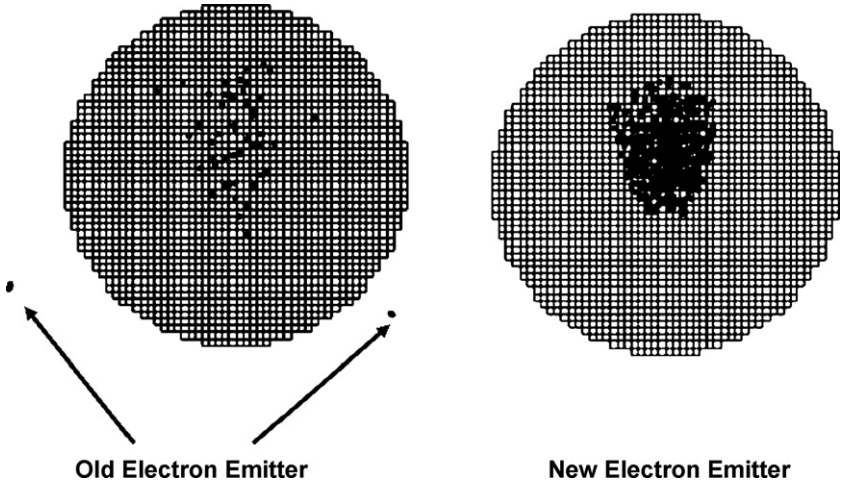

Fig. 3. Comparison of the simulated Cl^+ fragment ion beam obtained from dissociative ionization of $SiCl_4$ for a 3 eV excess kinetic energy of the Cl^+ ion (see text for details).

the interaction region and the detector, it is possible to identify the place where the ion hit a surface or was blocked.

The higher electron beam current from the new emitter and smaller interaction region result in significantly higher signal rates and a much more tightly focused product ion signature on the face of the MCP detector. This is shown in Fig. 3, where we simulated the Cl^+ fragment ion signal from the dissociative ionization of $SiCl_4$ (for an excess kinetic energy of 3 eV per Cl^+ fragment ion) on the face of the MCP detector for both the old and the new electron gun. In this simulation, the effect of the higher signal rate due to the more intense electron gun was not taken into account explicitly. Both simulations start with the same number of product ions in the interaction region. We note that the Cl^+ product ion beam obtained with the new electron emitter is much more tightly focused on the face of the MCP detector. Most importantly, the ion collection efficiency with the old emitter is already appreciably less than 100% for a 3 eV Cl^+ fragment ion from $SiCl_4$ as evidenced (i) by the fact that number of ions hitting the detector surface is considerably larger in the right diagram (new emitter) compared to the left diagram (a significant fraction of the Cl^+ ions generated by the old emitter are lost during ion transport through the apparatus and never reach the detector) and (ii) by the ions in the left diagram that "miss" the surface area of the MCP, whereas all product ions lie well within the cross sectional area of the MCP when the new electron emitter is employed (no ions are lost in transport and the ion collection efficiency is 100% in this case).

2.3. Test measurements

We tested the performance of the modified fast-beam apparatus by carrying out a series of test measurements using the rare gases (He, Ne, Ar, Kr, and Xe), for which the ionization cross sections (absolute values and cross section shapes) are well known and for N_2, where the significant excess kinetic energy of the N^+ fragment formed in the dissociative ionization process poses a serious challenge to the capabilities of the any apparatus.

The absolute ionization cross sections of the rare gases are known with higher accuracy (±4% for Ar, between ±5% and ±8% for He, Ne, and Kr and ±12% for Xe) than the cross section of any other atom or molecule [19]. The partial rare gas ionization cross sections of Freund and co-workers [5] obtained with the 'old' fast-neutral-beam apparatus are considered among the most reliable data (see, e.g., discussion in Ref. [19]). We remeasured the absolute single rare gas ionization cross sections in the new fast-neutral-beam apparatus in the following way. We determined (i) the shape of the Ar^+ single ionization cross section, which has a well-established shape with a very distinct feature around 50 eV and (ii) the ratios of the cross sections for the formation of all singly charged rare gas ions at a fixed energy of 70 eV relative to the Ar ionization cross section. This was done by determining the MCP count rate that corresponds to the established absolute Ar^+ cross section at 70 eV. On the basis of the rare gas ionization cross section ratios at 70 eV as obtained from Ref. [19], we then calculated the expected MCP count rates that correspond to the absolute He^+, Ne^+, Kr^+, and Xe^+ cross sections at 70 eV and measured the actual count rates. The agreement between our measured and calculated count rates was excellent, all values agreeing with each other well within the margins of error that can be expected based on the quoted accuracy of the underlying absolute cross sections.

Several groups have employed mass-selective techniques to measure partial ionization cross sections for the formation of N_2^+ and N^+ ions from N_2 (see, e.g., Peterson [20] and Freund et al. [21]). While the N_2^+ parent ions are formed with thermal or near-thermal kinetic energy, the dissociative ionization leading to N^+ produces fragment ions with a broad excess kinetic energy distribution [1] as evidenced by an N^+ appearance energy of about 30 eV, which is significantly higher than the thermochemical minimum energy of 24.3 eV required to produce N^+ from N_2 (N^+/N_2). We combined SIMION ion trajectory modeling for the formation of N^+ ions from N_2 in the modified fast-beam apparatus with measurements of all partial N_2 ionization cross sections. We simulated the N^+/N_2 ion distribution on the MCP detector with the excess kinetic energy as a free parameter and compared the simulated distribution with measured distributions. A comparison between the measured and simulated ion distributions on the face of the MCP detector reveals (at least qualitative) information about the actual excess kinetic energy distribution and provides a measure of the ion collection efficiency under various operating conditions. Up to an excess kinetic energy of 4.65 eV per N^+ ion, we could demonstrate a 100% N^+ ion collection efficiency. Subsequently, we carried out absolute ionization cross section measurements of N_2 in the modified fast-beam apparatus measuring the N_2^+ and ($N^+ + N_2^{++}$) partial cross sections as well as the respective appearance energies. The results agreed with the accepted cross section values to better than ±5% and to better than ±0.5 eV for the appearance energies.

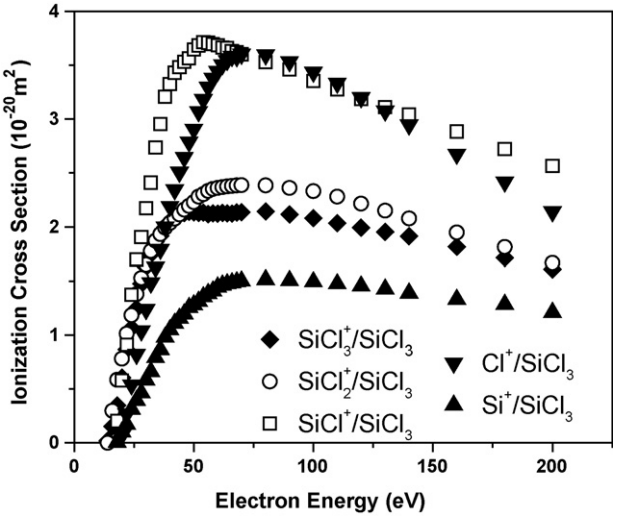

Fig. 4. Absolute partial cross sections for the formation of the singly charged ions $SiCl_3^+$ (diamonds), $SiCl_2^+$ (circles), $SiCl^+$ (squares), Cl^+ (inverted triangles), and Si^+ (triangles) as a function of electron energy from threshold to 200 eV. The absolute cross sections have margins of uncertainty of ±15% (see text), which are not shown.

3. Results and discussions

The results of the absolute partial ionization cross section measurements for the $SiCl_3$ free radical from threshold to 200 eV using the modified fast-beam apparatus are presented and discussed in this section. Fig. 4 shows the measured partial cross sections for the formation of the $SiCl_3^+$ parent ion and all singly charged fragment ions $SiCl_2^+$, $SiCl^+$, Si^+, and Cl^+. The partial ionization cross sections as well as the total single $SiCl_3$ ionization cross section are summarized in Table 1 for easy reference. Cross sections for the formation of doubly charged ions are not reported here, since the maximum values of the cross sections for formation of doubly charged ions from $SiCl_3$ are less than 0.1×10^{-20} m^2, similar to what was found earlier in the case of $SiCl_4$ [6] and for $SiCl_2$ and SiCl [7].

The partial ionization cross sections can be grouped into three categories according to their absolute magnitude: (i) the $SiCl^+$ and Cl^+ cross sections have the largest maximum cross section values (>3.5×10^{-20} m^2), (ii) the $SiCl_3^+$ and $SiCl_2^+$ cross sections have maximum values slightly exceeding 2×10^{-20} m^2, and (iii) the Si^+ cross section has a maximum value of about 1.51×10^{-20} m^2. The

Table 1
Absolute partial and total single electron-impact ionization cross sections for $SiCl_3$ as a function of electron energy from threshold to 200 eV

Electron energy (eV)	Ionization cross section ($\times 10^{-20}$ m^2)					
	$SiCl_3^+$	$SiCl_2^+$	$SiCl^+$	Si^+	Cl^+	Total (single)
12	–	–	–	–	–	–
14	0.01	–	–	–	–	0.01
16	0.15	0.30	–	–	–	0.45
18	0.35	0.58	0.20	0.004	–	1.13
20	0.60	0.78	0.58	0.10	0.07	2.13
22	0.87	1.01	0.91	0.17	0.27	3.22
24	1.07	1.18	1.37	0.31	0.54	4.47
26	1.24	1.38	1.70	0.39	0.82	5.53
28	1.47	1.53	1.90	0.46	1.04	6.40
30	1.63	1.65	2.17	0.58	1.24	7.27
32	1.75	1.78	2.41	0.66	1.48	8.07
34	1.86	1.87	2.73	0.79	1.62	8.88
36	1.92	1.93	2.95	0.86	1.79	9.46
38	2.00	1.99	3.21	0.98	2.00	10.17
40	2.05	2.04	3.32	1.04	2.19	10.64
42	2.07	2.08	3.43	1.11	2.34	11.03
44	2.11	2.11	3.48	1.15	2.51	11.37
46	2.13	2.16	3.53	1.20	2.64	11.65
48	2.14	2.19	3.56	1.25	2.79	11.94
50	2.13	2.23	3.64	1.28	2.90	12.19
52	2.12	2.28	3.68	1.31	3.07	12.47
54	2.13	2.30	3.71	1.35	3.18	12.68
56	2.12	2.33	3.71	1.38	3.30	12.84
58	2.12	2.35	3.70	1.41	3.38	12.96
60	2.12	2.36	3.68	1.44	3.44	13.05
62	2.13	2.37	3.66	1.46	3.50	13.13
64	2.12	2.38	3.66	1.47	3.54	13.17
66	2.12	2.38	3.63	1.48	3.58	13.19
68	2.13	2.38	3.62	1.49	3.58	13.21
70	2.14	2.39	3.60	1.50	3.60	13.22
80	2.14	2.39	3.53	1.51	3.59	13.16
90	2.11	2.36	3.46	1.50	3.53	12.97
100	2.08	2.33	3.35	1.49	3.43	12.69
110	2.03	2.28	3.28	1.47	3.33	12.40
120	1.99	2.21	3.19	1.45	3.19	12.04
130	1.95	2.15	3.11	1.43	3.07	11.71
140	1.91	2.08	3.04	1.39	2.94	11.36
160	1.82	1.95	2.88	1.33	2.67	10.65
180	1.71	1.81	2.72	1.28	2.41	9.95
200	1.61	1.67	2.56	1.21	2.14	9.19

parent $SiCl_3^+$ cross section curve has a threshold of about 12.3 eV and rises to its maximum of 2.14×10^{-20} m^2 at an electron energy of slightly below 50 eV. The cross section then declines slightly with increasing impact energy followed by a second maximum of similar magnitude at about 80 eV. Subsequently, the cross section curves gradually declines to about 1.6×10^{-20} m^2 at 200 eV. The $SiCl_2^+$ cross section, with a threshold of about 13 eV, rises in a fashion similar to $SiCl_3^+$ cross section, but exhibits only one maximum of 2.4×10^{-20} m^2 around 70 eV. The $SiCl^+$ cross section rises from a threshold of about 14.8 eV to a narrow maximum of 3.7×10^{-20} m^2 at about 55 eV and declines to a value of slightly less than 2.6×10^{-20} m^2 at 200 eV. The Cl^+ and Si^+ cross sections have both thresholds of just below 20 eV. The Cl^+ cross section has a fairly sharp maximum of 3.6×10^{-20} m^2 at 70 eV. By contrast, the Si^+ cross section has a broad maximum of 1.5×10^{-20} m^2 around 80 eV and shows a much more gradual decline towards higher impact energies. The shape of the $SiCl_3^+$ cross section with a double-maximum structure is similar to what was observed earlier for selected partial $SiCl_4$, $SiCl_2$, and SiCl cross sections [6,7] as well as for some partial cross sections of other Cl-containing molecules, such as $TiCl_4$ [22], and Cl_2 [23]. The low-energy maximum may be indicative of the presence of indirect ionization channels such as autoionization. We note that the observed appearance energies for the various ions are very close to the known ionization energy in the case of the $SiCl_3^+$ parent ion and the thermochemical minimum energies required for the formation of the various fragment ions. This indicates that the fragment ions are formed with little excess kinetic energy.

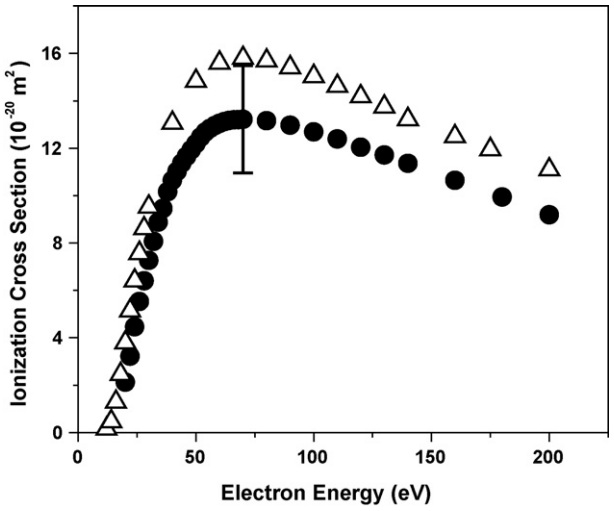

Fig. 5. Absolute total single $SiCl_3$ ionization cross section as a function of electron energy from threshold to 200 eV, present experiment (circles) and calculated cross sections using the DM formalism (triangles).

We are only aware of one calculation of the $SiCl_3$ total single ionization cross section, namely a calculation based on the semi-empirical Deutsch–Märk (DM) formalism [2]. Fig. 5 shows the experimentally determined total single $SiCl_3$ ionization cross section (which is obtained as the sum of all the partial cross sections for the formation of singly charged ions) in comparison with the calculated total single DM cross section for $SiCl_3$. The agreement between measured and calculated total single ionization cross sections is very good in terms of the cross section shape, but less satisfactory in terms of the absolute cross section magnitude. The calculated cross section exceeds the measured cross section at impact energies above 30 eV. The discrepancy reaches about 20% in the region of the cross section maximum. We note that the overall uncertainty in the experimentally determined cross section is about ±17% at 70 eV and is given by the sum of the uncertainties in the relative partial cross sections (added in quadrature) and the uncertainty in the absolute cross section calibration. The level of agreement between calculated and experimentally determined $SiCl_3$ cross section is similar to what was found for other polyatomic molecules (see, e.g., Deutsch et al. [2]). We note, however, that by contrast the agreement between calculated and experimentally determined (maximum) cross section for $SiCl_4$ [6] and for $SiCl_2$ and SiCl [7] was better than 5%.

4. Conclusions

The fast-beam apparatus that has been used extensively for ionization cross section measurements in our group for more than 15 years was modified by introducing a new high-current electron emitter and a position-sensitive MCP detector. Experiments using well-established ionization cross sections in conjunction with extensive ion trajectory simulations were carried out to verify the performance of the modified fast-neutral-beam apparatus. Using the modified apparatus, we measured absolute partial cross sections for the formation of all singly charged ions following electron impact on $SiCl_3$ from threshold to 200 eV. Maximum cross section values range from 1.5×10^{-20} m^2 to 4×10^{-20} m^2. Several partial cross section curves show a prominent structure around 30 eV, which may be indicative of the presence of indirect ionization channels such as autoionization. A comparison between the

experimentally determined total single $SiCl_3$ cross section and a calculated cross section using the DM formalism shows that the calculated cross section lies systematically above the experimental data. The discrepancy of 20% is similar to what was found previously for other polyatomic molecules, but is larger than the excellent agreement that was found for $SiCl_4$, $SiCl_2$, and SiCl [6,7].

A comparison of the $SiCl_3$ ionization cross sections with the ionization cross sections for the $SiCl_4$ parent molecule [6] and the $SiCl_2$ and SiCl compounds [7] reveals the following findings:

(1) the maximum value of the total single ionization cross section increases with increasing number of Cl-atoms in the target from 8×10^{-20} m^2 for SiCl to about 20×10^{-20} m^2 for $SiCl_4$;
(2) all four compounds have stable parent ions and the parent ionization cross sections are quite large (compared to those of other halogen-containing polyatomic molecules of similar molecular structure) with maximum values from 2×10^{-20} m^2 for $SiCl_3$ to almost 4×10^{-20} m^2 for $SiCl_4$, with both $SiCl_2$ and SiCl having maximum cross sections around 2.5×10^{-20} m^2;
(3) both atomic fragment ions Cl^+ and Si^+ are formed with comparatively large cross sections for all four species, which underscores the importance of these species in plasma processing applications;
(4) essentially all fragment ions resulting from the dissociative electron-impact ionization of the four compounds $SiCl_x$ (x = 1–4) are formed with little excess kinetic energy.

Acknowledgments

It is our great pleasure to contribute this article to this Special Issue of the IJMS honoring Prof. Zdenek Herman. Long before "interdisciplinary and multidisciplinary research" became buzz words, Zdenek carried out research that seamlessly and effortlessly crossed the boundaries between physics and chemistry and applied methods and techniques from both disciplines to provide insights into issues that neither physicists nor chemists working within the confines of their respective discipline felt comfortable attacking. We are humbled to join the scientific community in recognizing Zdenek Herman as one of the pioneers of inter- and multidisciplinary research in physics and chemistry.

This work was partially supported by the Chemical Sciences, Geosciences, and Biosciences Division, Office of Basic Energy Sciences, U.S. Department of Energy.

References

[1] T.D. Märk, G.H. Dunn (Eds.), Electron Impact Ionization, Springer Verlag, Vienna, 1985.
[2] H. Deutsch, K. Becker, S. Matt, T.D. Märk, Int. J. Mass Spectrom. 197 (2000) 37, and references therein to earlier work.
[3] H.U. Poll, C. Winkler, T.D. Märk, Int. J. Mass Spectrom. Ion Proc. 112 (1992) 1.
[4] C.J. Cook, J.R. Peterson, Phys. Rev. Lett. 9 (1962) 164.
[5] R.C. Wetzel, F.A. Biaocchi, T.R. Hayes, R.S. Freund, Phys. Rev. A 35 (1987) 559.
[6] R. Basner, M. Gutkin, J. Mahoney, V. Tarnovsky, H. Deutsch, K. Becker, J. Chem. Phys. 123 (2005) 05313.
[7] J. Mahoney, V. Tarnovsky, K. Becker, Euro. J. Phys. D 46 (2008) 289.
[8] D. Bloor, R.J. Brook, M.C. Flemings, S. Mahajahn, R.W. Cahn, Ion Etching and Plasma Etching of Silicon, Pergamon, New York, 1993.
[9] V.M. Donnelly, J. Appl. Phys. 79 (1996) 9353.
[10] S.J. Ullal, T.W. Kim, V. Vahedi, E.S. Aydil, J. Vac. Sci. Technol. A 21 (2003) 589.
[11] R.J. Shul, S.J. Pearton, Handbook of Advanced Plasma Processing Techniques, Springer, Berlin Heidelberg, 2000.
[12] Y. Fujimura, S. Jung, H. Shirai, Jpn. J. Appl. Phys. 40 (2001) 1214.
[13] I.I. Negulescu, S. Despa, J. Chen, B.J. Collier, M. Despa, A. Denes, M. Sarmadi, F.S. Denes, Text. Res. J. 70 (2000) 1.
[14] L.M. Blinov, A.G. Golovkin, L.I. Kaganov, V.B. Oparin, A.A. Razhavski, A.M. Shterenberg, V.V. Volodko, V.I. Zyn, Plasma Chem. Plasma Process 18 (1998) 509.
[15] J. Mahoney, M. Gutkin, V. Tarnovsky, K. S Becker, in: Proceedings of the 15th International Conference on Electron-Molecule Collisions and Swarms Reading, UK, 2007, J. Phys. Conf. Ser. 115 (2008) 012010.
[16] V. Tarnovsky, K. Becker, Z. Phys. D 22 (1992) 603.
[17] J. Lopez, M. Gutkin, V. Tarnovsky, K. Becker, Int. J. Mass Spectrom. 225 (2003) 25.
[18] Simion 3D, Version 7.0, Idaho National Engineering and Environmental Laboratory, Idaho Falls, ID 83415.
[19] R. Rejoub, B.G. Lindsay, R.F. Stebbings, Phys. Rev. A 65 (2002) 042713.
[20] J.R. Peterson, in: M.R.C. McDowell (Ed.), Proceedings of the III ICPEAC, London, 1963, North Holland Publication, Amsterdam, 1964, p. 465.
[21] R.S. Freund, R.C. Wetzel, R.J. Shul, Phys. Rev. A 41 (1990) 5861.
[22] Basner, M. Schmidt, V. Tarnovsky, H. Deutsch, K. Becker, Thin Solid Films 374 (2000) 291.
[23] R. Basner, K. Becker, New J. Phys. 6 (2004) 118.